1   **Title:** Resistant potato starch fuels beneficial host-microbe interactions in the gut

2   **Authors:** Julian Trachsel[1,2], Cassidy Briggs[1,3], Nicholas K. Gabler[4], Heather K. Allen[1] #, Crystal

3   L. Loving[1] #

4   **Author Affiliations:**

5   1 Food Safety and Enteric Pathogens Research Unit, National Animal Disease Center,

6   Agricultural Research Service, Ames, IA, 50010, USA

7   2 Interdepartmental Microbiology Graduate Program, Iowa State University, Ames, IA, 50010,

8   USA

9   3 Iowa State University College of Veterinary Medicine Summer Scholar Research Program

10   4 Department of Animal Science, Iowa State University, Ames, IA, 50011

11   **Keywords:** resistant starch, mucosa, microbial accessible carbohydrates, butyrate, microbiota,

12   microbial respiration, prebiotics, t-regulatory cells, colonization resistance, mucosal barrier,

13   immune tolerance.

14

15

16

17

18

19

20 **Abstract**

21 Interactions between diet, the microbiota, and the host set the ecological conditions in the gut

22 and have broad implications for health. Prebiotics are dietary compounds that may shift these

23 conditions towards health by promoting the growth of beneficial microbes. Pigs fed a diet

24 amended with 5% resistant potato starch (RPS) exhibited alterations associated with gut health

25 relative to swine fed an unamended diet (CON). RPS intake increased abundances of anaerobic

26 *Clostridia* in feces and several tissues, as well as intestinal concentrations of butyrate.

27 Functional gene amplicons suggested bacteria similar to *Anaerostipes hadrus* were stimulated by

28 RPS intake. The CON treatment exhibited increased abundances of several genera of

29 *Proteobacteria* (which utilize respiratory metabolisms) in several location. RPS intake increased

30 the abundance of regulatory T cells in the cecum, but not periphery, and cecal immune status

31 alterations were indicative of enhanced mucosal defenses. A network analysis of host and

32 microbial changes in the cecum revealed that regulatory T cells positively correlated with

33 butyrate concentration, luminal IgA concentration, expression of IL-6 and DEF1B, and several

34 mucosa-associated bacterial taxa. Thus, the administration of RPS modulated the microbiota and

35 host response, improved cecal barrier function, promoted immunological tolerance, and reduced

36 the niche for bacterial respiration.

37 **Importance**

38 The gut microbiota is central to host health. Many disease states and disorders appear to

39 arise from interactions between the gut microbial community and host immune system. As a

40 result, methods and interventions to support the growth and activity of beneficial gut microbes

41 are being actively pursued. Feeding the gut microbiota with dietary compounds, known as

42 prebiotics, is one of the most promising ways to support gut health. Here we describe a

43   successful prebiotic intervention in weaning swine, a relevant translational model for human

44   health. This work unites microbial and immunological data and demonstrates one way a

45   prebiotic intervention can play out for the benefit of the host.

46

47   **Introduction**

48   Dietary prebiotics, such as resistant starches, provide an attractive alternative to

49   antibiotics for improved animal health, including humans (1). Resistant starches are compounds

50   that are not digested by the host in the small intestine, thereby arriving in the large intestine as

51   microbial-accessible carbohydrates. Bacteria that consume resistant starches are normal members

52   of the microbiota and are associated with intestinal health (2). Without access to diet-derived

53   carbohydrates, bacteria will harvest host-derived sugars from the intestinal mucus layer,

54   compromising barrier function (3). However, if dietary carbohydrates are accessible, bacteria

55   will ferment these compounds and release beneficial metabolites, particularly short-chain fatty

56   acids (SCFAs). Host cells consume the vast majority of microbial-produced SCFAs, fueling

57   intestinal homeostasis (4-6).

58   The SCFA butyrate is a central metabolite for maintaining intestinal homeostasis. It is

59   the preferred fuel source for colonocytes, which oxidize butyrate and consume oxygen. This

60   oxygen consumption lowers the oxygen potential of the epithelia, reducing the amount of

61   electron acceptors available for bacterial respiration (4, 7-9). Furthermore, butyrate can help to

62   limit immune activation by enhancing mucosal barrier function and immunological tolerance,

63   reducing the secretion of immune-derived reactive oxygen and nitrogen species, which also can

64   be used in microbial respiration. Butyrate benefits mucosal barrier function by stimulating

65   increased secretion of mucus, antimicrobial peptides (10), and IgA (6), therefore preventing the

66   translocation of intestinal bacteria that would elicit an immune response. Second, butyrate can

67   induce a more tolerant immune phenotype through the generation of several regulatory immune

68   cell types (11). In total, butyrate-driven changes to the gut microenvironment limit the niche for

69   microbes with respiratory metabolisms (8, 9), allowing microbes that specialize in fermentation

70   to outcompete those that respire, such as *Campylobacter, Salmonella,* and *Escherichia* species

71   (4, 7).

72   Dietary intake of resistant starches may make the intestinal ecosystem less hospitable for

73   potential pathogens and limit the negative impact of weaning on mammalian health. For

74   example, feeding resistant potato starch (RPS) to nursery-aged piglets enhances some markers of

75   gut health (12). However, the mechanisms by which RPS supports intestinal health in the

76   weaned mammal are poorly defined. The results reported here suggest that dietary RPS

77   encouraged beneficial host-microbe interactions in the hindgut ecosystem. Specifically, RPS

78   stimulated bacterial food webs with functional activities for increased SCFA and butyrate

79   production, which caused subsequent changes in the host intestinal immune status. Immune

80   changes included increased T-regulatory cell types in the cecal tissues, markers of enhanced

81   mucosal barrier function, and reduced amounts of potentially harmful bacteria known to utilize

82   respiratory metabolisms. Collectively, dietary RPS given to pigs at weaning modulated bacterial

83   populations and host immune status to a state associated with enhanced intestinal health.

84   **Results**

85   ***No overt differences in health were observed between the two treatment groups***

86   All pigs appeared healthy throughout the study with no obvious differences in health or

87   behavior observed between the groups. No significant differences in weights were observed

88   either at weaning or necropsy. No gross pathology was observed at necropsy, nor were

89   microscopic pathological changes noted in sections of cecal tissues. These data suggest that all

90   animals in this study were healthy regardless of treatment.

91   ***Bacterial community structure and metabolites differed between the two treatment groups***

92   Both the CON and RPS groups showed similar weaning-related changes in their bacterial

93   communities; however, the communities of the groups became less similar over time. Group

94   fecal bacterial community structures did not differ significantly until day 15, which was

95   associated with a recent dietary phase change (12 days post-weaning), marked by a decrease in

96   the amount of dietary lactose (**Figure 1A, Table S3**). By day 21 the two treatment groups had

97   significantly different fecal bacterial community structures. Group differences in community

98   structures were seen in both the 16S rRNA gene sequence-based analysis, as well as the *but-*

99   based analysis. The size of these effects were driven in part by community dispersion (**Figure**

100   **1B**). The 16S rRNA gene-based analysis showed significantly less intra-group variability among

101   the RPS-fed pigs compared to the CON-fed pigs at day 21, and the bacterial community structure

102   of both groups became less dispersed as they matured (**Figure 1B, Table S4**). These results

103   suggest that weaning-associated changes in bacterial communities were more profound than

104   RPS-associated changes, and that RPS intake did not immediately affect the composition of the

105   microbiota, but over time, significantly affected both the overall community composition and the

106   intragroup variability as these communities matured.

107   Twenty-one days after weaning, the structure of the microbiota was significantly different

108   between the CON and RPS groups at multiple intestinal locations. The 16S rRNA gene-based

109   analyses tended to show greater differences than the *but* gene-based analyses (**Figure 2A, B and**

110   **Table S3**). The tissue-associated bacterial communities exhibited the same dispersion trend as

111   the fecal communities, with the communities in tissues from RPS-fed pigs exhibiting less group

112   dispersion (**Table S4**). These data suggest that the effects of RPS intake on bacterial

113   communities were not limited to one tissue or location, but bacterial populations throughout the

114   intestinal tract were similarly impacted resulting in higher intragroup similarity in the RPS

115   animals.

116   Short-chain fatty acid (SCFA) concentrations in cecal and fecal samples collected at 21-

117   days post-weaning were evaluated to investigate whether the changes in bacterial communities

118   had an impact on microbial metabolic output. Aligning with the changes in microbial community

119   structure, the CON and RPS-fed pigs had differing SCFA profiles (**Fig 2C**). Pigs fed RPS had

120   higher amounts of butyrate in both the cecum and feces (p=0.05 & p=0.05), higher levels of

121   caproate in both the cecum and feces (p=0.07 & p=0.001), lower levels of propionate in the

122   cecum (p=0.05), higher amounts of lactate in the cecum (p=0.09), and lower levels of lactate in

123   the feces (p=0.02). Total SCFA concentrations in cecal contents were not different between the

124   treatments, but total fecal SCFAs were significantly increased in the RPS group (p=0.03).

125   Collectively, dietary RPS modulated bacterial community structure in the distal gut, and these

126   community differences were associated with different SCFA production levels.

127   ***Differentially abundant bacterial genera between the treatment groups***

128   At day 21 post-weaning, many bacterial genera were significantly differentially abundant

129   at several intestinal sites between the treatments (**Figure 3**). Several genera were consistently

130   associated with each respective treatment in most sampling locations. Pigs fed RPS had

131   significantly increased levels of *Terrisporobacter, Sarcina,* and *Clostridium sensu stricto 1*

132 compared to CON-fed pigs. CON-fed pigs had a significant enrichment of *Mucispirillum,* as well

133 as occasional enrichment of various *Proteobacteria* genera such as *Helicobacter, Sutterella,* and

134 *Campylobacter* in different tissues, and many of the genera enriched in CON group harbored

135 members known to utilize respiratory metabolisms (13-16). One 16S rRNA gene OTU,

136 OTU00087, was largely responsible for the differential abundance of the genus *Clostriduim*

137 *sensu stricto 1* between the two treatment groups. This OTU was greatly enriched in samples

138 from pigs fed RPS, regardless of time point and site (**Figure 4**). Sequences from OTU00087

139 most closely matched *Clostridium chartatabidum*; organisms similar to this bacterial species are

140 shown to tightly bind starch granules and have been isolated from human feces(17) . This

141 suggests that certain bacterial species may occupy the same nutritional niche in many different

142 hosts.

143   Similar to the 16S rRNA gene sequence data, many *but* gene-based OTUs were

144 differentially represented between the two groups (**Figure 5**). RPS intake was consistently

145 associated with a greater abundance of *but* OTUs whose sequences most closely matched to

146 those from *Anaerostipes hadrus,* as well as a *but* OTU whose sequences most closely matched an

147 organism detected in metagenomes from human feces (*but* OTU0067). Intestinal samples from

148 CON group had significant enrichments of *but* OTUs whose sequences most closely matched

149 genes from *Pseudobutyvibrio* and *Helicobacter*. Collectively, these results suggest that

150 particular butyrate-producing bacteria were enriched by RPS intake, and their metabolic

151 activities were likely responsible for increased butyrate concentrations detected in the intestinal

152 samples from these animals.

153 ***Bacterial food webs associated with the dietary treatments***

154   To investigate bacterial food webs associated with the increased SCFA levels in the RPS-

155   fed animals, we constructed a correlation network using *but* and 16S rRNA gene OTUs. The

156   network was filtered such that all nodes in the network were differentially abundant between the

157   two groups as determined by DeSeq2, and so the network represented the food webs that were

158   most different between the treatment groups. Nodes enriched in the RPS treatment group

159   clustered into one primary subnetwork, whereas nodes enriched in the CON group clustered into

160   two smaller subnetworks (**Figure 6**). The primary subnetwork enriched in RPS-fed pigs

161   represented bacterial OTUs likely involved in the fermentation of RPS to SCFAs. Bacterial

162   species comprising the RPS-associated network are known to be involved in the breakdown and

163   fermentation of dietary starches, such as *Eubacterium rectale, Mitsuokella* spp., *Prevotella* spp.,

164   and *Bifidobacterium* spp (18). These organisms can degrade RPS into small polysaccharides or

165   other metabolic inputs, such as lactate, which are then an available carbon source for other

166   bacteria. Lactate-consuming and butyrate-producing bacteria were also present in the RPS-

167   associated network, including *Megasphaera elsdenii*. These results suggest that dietary RPS

168   supplementation enriched for a bacterial food web that degraded dietary RPS and produced

169   SCFAs via bacterial fermentation.

170   ***Differential host response with dietary RPS***

171   To investigate the impact of dietary RPS on immune status, and to correlate detected

172   immune changes with bacterial community alteration, T cell populations in the cecum, ileocecal

173   lymph node, and peripheral blood were phenotyped by flow cytometry. From this analysis we

174   did not detect a significant difference in the abundance of CD3$^+$ cells in any sample type between

175   treatment groups, and the lack of change to the number of CD3$^+$ cecal cells with dietary RPS was

176   supported by IHC results (**Figure S3**). In the cecum, less than 1% of the CD3$^+$ cells expressed

177   the γδ T cell receptor (**Figure S2**), indicating that nearly all of the T cells in the cecum were αβ T

178   cells.

179   Subsequent analysis of cecal T cell populations revealed distinct changes associated with

180   dietary treatment. A panel of antibodies against CD3, CD4, CD8α, CD25, and FoxP3 were used

181   to simultaneously identify 16 distinct T cell populations (**Table S5**). The relative abundance of

182   each cell type was reported as a percent of the total $CD3^+$ cells, generating a community data

183   matrix for ecological analyses. No significant differences between groups were observed in T

184   cell communities in the ileocecal lymph node or peripheral blood; however, a significant

185   difference in overall cecal T cell community structure was detected between treatment groups

186   (**Figure 7A**) (PERMANOVA p=0.001, F=12.06). Additionally, the evenness of the cecal T cell

187   communities in CON animals was significantly reduced, meaning these communities tended to

188   be dominated by a few cell types (**Figure 7B,** p = 0.02). Several types of cecal T cells were

189   differentially abundant between the treatments (**Figure 7C**). More specifically, we observed an

190   increase in several $CD8α^+$ populations and a relative decrease in $FoxP3^+$ cells in CON animals.

191   These data suggest that animals fed RPS had increased abundances of T regulatory cell types

192   associated with immune tolerance; however, these changes were limited to the cecal mucosa.

193   In addition to differences in the cecal T cell populations, significant differences in the

194   expression of genes important for barrier function were detected in the cecal mucosa.

195   Significantly greater expression of MUC2 and IL6 was observed (p=0.03 and p=0.03), as well as

196   a trend towards increased expression of DEF1B (p=0.16) in the RPS-fed group compared to the

197   CON group (**Figure 8A**). Intestinal IgA is another important host-produced factor that enhances

198   intestinal barrier function; therefore, cecal luminal contents were assayed for total IgA

199   concentration. RPS-fed pigs trended towards increased cecal luminal IgA at necropsy (p=0.08)

200   (**Figure 8B**). No increase in the number of IgA$^+$ cells in cecal tissues was detected, (**Figure S3**)

201   suggesting increased secretion of IgA from plasma cells in the cecum.

Bacterial members and metabolites correlated with immune status

203   To investigate relationships among bacterial membership, bacterial function, and host

204   immune status in the cecum, a correlation network was constructed using the relative abundance

205   of cecal cells [both CD3$^+$ and CD3$^-$ cell types were used in this analysis, (**Table S6**)], cecal 16S

206   rRNA gene sequence diversity, cecal SCFA concentrations, cecal tissue gene expression, and

207   luminal IgA concentrations (**Figure 9**). The results showed one discrete subnetwork associated

208   with each respective treatment group. The subnetwork associated with pigs fed RPS (labeled

209   subnetwork-A) was composed of features associated with immune tolerance, mucosal barrier

210   function, and anaerobic microbial fermentation. Classic T-regulatory (CD3$^+$CD4$^+$CD8α$^-$

211   CD25$^+$FoxP3$^+$) cells formed a central node in the RPS subnetwork along with several other

212   CD3$^+$FoxP3$^+$ cell-types. Concentrations of the SCFAs butyrate, caproate, and valerate correlated

213   with these regulatory T cells. Bacterial OTUs in the RPS subnetwork belonged to groups known

214   for anaerobic fermentation, and several OTUs corresponded to known butyrate-producing

215   bacterial groups, such as the genus *Megasphaera* and the family *Ruminococcaceae.* In addition,

216   subnetwork-A contained nodes associated with an enhanced mucosal barrier: DEF1B, and IL-6

217   expression, and high luminal IgA concentrations.

218   The subnetwork associated with the CON diet (labeled subnetwork-B) was composed of

219   markedly different features defined by immune activation, cytotoxic T cells, and bacteria capable

220   of respiration. Not all of the features of subnetwork-B were significantly enriched in the CON

221   pigs. Only cytotoxic T cells (both CD25+ and CD25-), propionate, a *Succinivibrio* OTU, and a

222   *Mucispirillum* OTU were enriched in the CON diet.   The core of subnetwork-B was composed

223   of highly interconnected nodes, mainly cells expressing CD25 and a *Campylobacter* OTU,

224   suggesting T cell activation and conditions conducive to microbial respiration. Several of the

225   OTUs in subnetwork-B belong to the *Proteobacteria* phylum, members of which are known to

226   use respiratory metabolisms (19). These results suggest that dietary RPS enhanced bacterial

227   production of SCFAs that benefited host health by promoting epithelial barrier function,

228   increased immune tolerance, and a reduced niche for microbial respiration relative to CON-fed

229   pigs.

230   **Discussion**

231   RPS is an accessible metabolic substrate for intestinal microbes and can lead to increased

232   production of SCFAs, particularly butyrate, which have beneficial effects on the gastrointestinal

233   system (20). Our results showed increased concentrations of cecal butyrate and lactate in RPS-

234   fed animals compared to the CON animals. In the distal gut, lactate is converted to butyrate (21),

235   and the lactate observed in the cecum was likely converted to butyrate during colonic passage as

236   fecal lactate concentrations were very low. Supporting this idea, we observed an enrichment of

237   butyrate–producing bacteria known to consume lactate, including *Anaerostipes hadrus* and

238   *Megasphaera elsdenii,* in RPS-fed animals. Butyrate is well established as a bacterial metabolite

239   of central importance for intestinal homeostasis that supports many aspects of gut health,

240   including reducing the mucosal niche for bacterial respiration (7), increasing barrier function (4,

241   22), and encouraging an appropriate immune response skewing towards T cell tolerance of

242   symbiotic microbes (23, 24).

243   The effects of prebiotics such as RPS are mediated through the microbiota, consequently

244   the impact can vary greatly depending on the initial composition of intestinal bacterial

245   communities. The large inter-individual variation present in the intestinal microbiota of

246   mammals is well documented, swine included (25).   Several studies investigating dietary

247   resistant starch have found that prebiotic responders and non-responders can be grouped by the

248   presence of certain microbial members (18). This phenomenon was also observed in the present

249   study, as we detected variation in the response of individual pigs to RPS. Therefore, to optimize

250   the effect of dietary prebiotics it may be necessary to ensure that the appropriate microbial food

251   webs are present in the host. One study suggests that co-administration of resistant starch and a

252   probiotic strain of *Bifidobacteria* spp. produced more desirable health outcomes than resistant

253   starch alone (26). Our work identifies swine gut microbiota members that could be co-

254   administered alongside RPS to potentially enhance its beneficial effects.

255   RPS-associated bacterial food webs were composed of organisms known to use

256   fermentative metabolisms. Well-known fermenters such as *Bifidobacteria* spp. and

257   *Faecalibacterium* spp. were enriched in the RPS-fed animals and are associated with intestinal

258   health in humans (27), and other studies have shown increased abundance of these genera in pigs

259   fed resistant starch (2, 28). Some genera enriched in the RPS-fed animals are not well

260   characterized for their health benefits. For example, members of the genus *Clostridium sensu*

261   *stricto 1* are not generally associated with positive health outcomes; however, our data suggest

262   that members of this genus may be important for resistant starch degradation in the distal gut.

263   Many of the differences between the treatment groups were likely a result of feedback

264   interactions between intestinal bacterial metabolites and host tissues. Butyrate (and other SCFAs)

265   produced by gut bacteria is oxidized by host tissues, thereby limiting the amount of oxygen

266   available at the mucosa (7). This establishes a mucosal environment favoring microbial

267   fermentation over respiration, and therefore more SCFA production. Increased mucosal tolerance

268   additionally limits the release of immune-associated electron acceptors (8). In total these effects

269   limit the niche for microbial respiration, and the types of bacteria enriched in the RPS-fed

270   animals compared to the CON-fed animals are consistent with this model.

271   Increases in beneficial bacterial populations and metabolites in the RPS-fed animals were

272   associated with positive impacts on the mucosal barrier as well as increased immune regulatory

273   cells in the cecum. The results showed that RPS-associated microbial changes enhanced the

274   mucosal barrier by increasing the expression of MUC2, IL-6, and DEFB1 in the cecal mucosa.

275   IL-6 has recently been shown to be critical for maintaining the mucosal barrier (29) and has also

276   been shown to be important for strong IgA responses (30).   T cell subtypes, in particular T-

277   regulatory cells (T-regs), and indicators of intestinal health and mucosal barrier function

278   significantly correlated with microbial butyrate and caproate production, as well as several

279   anaerobic *Clostridial* OTUs in the cecal mucosa of the RPS-fed animals. Butyrate is known to

280   induce *de novo* generation and expansion of peripheral T-regs (reviewed in Zeng et. al (23)),

281   which are critical for intestinal homeostasis and gut barrier function (31). T-regs moderate

282   immune responses to commensal microbes, reducing intestinal inflammation and subsequent

283   mucosal availability of immune-derived electron acceptors, thereby limiting microbial

284   respiration (7). T-regs can promote mucosal IgA responses, helping the host exert control over

285   its microbial partners (23, 32, 33), and cecal luminal IgA levels were increased in RPS-fed pigs

286   and correlated with the abundance $CD4^+$ T-regulatory cells. $CD8\alpha^+$ T-regulatory cells $(CD4^-$

287   $CD8\alpha^+ CD25^+ FoxP3^+)$ are less well studied than $CD4^+$ T-regs, but recent work indicates they are

288   an important regulatory cell type in humans and mice (34), and we detected these cells in the

289   cecum of pigs.   Though their direct role in intestinal health is unclear, the network analysis

290   suggests that animals with greater relative abundance of $CD8^+$ T-regs correlated with greater

291   expression of DEFB1.

292   Though they were healthy, the CON group exhibited markers of reduced immune

293   tolerance and greater abundances of potentially invasive bacteria in their mucosal tissues.

294   Specifically, CON-fed animals had more cytotoxic T cells (CD8α$^+$ cell types) compared to RPS-

295   fed pigs, although they were unlikely active given the lack of pathological changes in the cecum.

296   Similarly, bacteria enriched in the CON animals have previously been associated with intestinal

297   inflammation, dysbiosis in humans and mice (35), and utilize respiration as their preferred

298   metabolism. In particular, members of the genus *Mucispirillum* have been shown to thrive in

299   inflamed, oxygenated mucosal environments (16). Our results showing correlations between the

300   abundance of *Mucispirillum* and cytotoxic T cells suggest that an immune cell activity may play

301   a role in expanding the niche for this organism in the CON pigs. Similarly, we detected

302   enrichment of *Helicobacter* 16S rRNA in the cecum and feces from CON-fed animals. Bacteria

303   from this genus can be facultative intracellular pathogens (36) , and it has been proposed that

304   non-*H. pylori Helicobacter* species may be a cause of irritable bowel disease (IBD) in humans

305   (29). These observations suggest that though the CON pigs lacked distinct pathology, the

306   mucosae of these animals were more amenable to colonization by potentially pathogenic

307   organisms that utilize respiratory metabolisms, relative to the RPS pigs.

308   Local intestinal inflammatory responses have previously been shown to occur in swine

309   early in weaning (37) , and though no overt inflammation was observed in these tissues in the

310   current study, we detected immune cell types associated with recent immune activity in both

311   treatment groups. In the cecal tissue network analysis, many nodes residing in subnetwork B

312   were equally represented in both the CON and RPS groups. For example, double-positive

313   (CD4$^+$CD8α$^+$) CD25$^+$ T cells were prominent members of subnetwork B and were not

314   differentially abundant between treatments; these cells have been shown to be common in swine

315   and represent activated, memory effector cells (38). Interestingly, a *Campylobacter* OTU, was

316   correlated with the abundance of these cells and several other CD25$^+$ cell types. This observation

317   suggests that certain bacterial groups, particularly *Proteobacteria,* may benefit from the local

318   environmental changes associated with recent immune activity, such as the release of reactive

319   nitrogen or oxygen species. While the memory cells may not be the source of reactive nitrogen

320   or oxygen species, their presence indicates prior perturbation of the mucosal site. The idea that

321   *Proteobacteria* thrive using products of the immune response is well established for *Salmonella*

322   in mice (8, 9) and our data suggest that this model warrants further investigation for other

323   bacterial species and hosts.

324   **Conclusions**

325   This study demonstrated that dietary intake of RPS had beneficial impacts on the

326   intestinal health status of weaning pigs, including increased markers of mucosal barrier function,

327   immune tolerance, and increased abundances of potentially beneficial bacterial populations. Our

328   study revealed the specific bacterial interactions involved in the bacterial breakdown of resistant

329   potato starch, and identified specific bacterial groups that could be co-administered with RPS to

330   enhance its effects. Additionally, this work revealed specific correlated changes between the

331   commensal microbiota and the mucosal immune system that can be used to inform future

332   strategies to modulate the microbiota to support health. These data provide valuable insights into

333   the host-microbe interactions in the intestinal mucosa of swine, furthering our knowledge of the

334   mammalian hindgut ecosystem. Finally, pigs are recognized as a relevant translational model for

335   human health, and research to enhance intestinal health in pigs provides insights for enhancing

336   human health as well.

337   **Materials and Methods**

338   *Experimental design*

339   Ten pregnant, Large White crossbred sows were delivered two weeks prior to farrowing,

340   and farrowed onsite. At 14 days-of-age, piglets were offered non-amended Phase 1 starter diet

341   (Table S1). At 21 days-of-age, piglets were weaned, and separated into two treatment groups.

342   Treatment groups consisted of two pens of seven piglets for a total of 14 piglets in each

343   treatment group, each group had equal representation from all litters. The control group (CON)

344   continued to receive non-amended Phase 1 Starter Diet. The treatment group was fed Phase 1

345   Starter Diet amended with 5% raw potato starch (RPS; MSP Starch Products Inc., Carberry,

346   Manitoba, Canada). At 12 days post-weaning (33 days-of-age), the CON group was switched to

347   non-amended Phase 2 Diet and the RPS group switched to Phase 2 Diet amended with 5% raw

348   potato starch (Table S1). At 21 days post-weaning (42 days-of-age), seven piglets from each

349   group (3 from one pen and 4 from a second pen) were humanely euthanized by injection of

350   sodium pentobarbital (Vortech Pharmaceuticals). All animal procedures were performed in

351   compliance with the National Animal Disease Center Animal Care and Use Committee

352   guidelines and review.

353   *Sample Collection*

354   Piglets were weighed at weaning and necropsy. Fecal samples were collected at 0, 12, 15,

355   19, and 21 days post-weaning. Feces were collected fresh and transported on ice, aliquoted for

356   downstream applications, and stored at -80 °C. Prior to euthanasia, peripheral blood was

357   collected into sodium citrate cell-preparation tubes (BD Pharmingen). At necropsy, cecal

358   contents were collected into RNALater and stored at 4 °C until RNA extraction, and snap frozen

359   and stored at -80 °C. Sections of cecal tissue were gently rinsed with phosphate-buffered saline

360   (PBS) and the mucosae were scraped with a sterile cell lifter. One portion of mucosal scrapings

361   was immediately stored in RNALater at 4 °C for host RNA extraction and another frozen at -80

362   °C for bacterial DNA extraction. Ileocecal lymph node and sections of cecal tissue were

363   collected in the appropriate buffer on ice and immediately processed for flow-cytometry.

Immunohistochemical Staining (IHC)

365   Fresh cecal tissues were formalin-fixed and sections prepared using standard histological

366   techniques. Details for CD3 and IgA staining are available in the supplement. Slides were

367   scanned into Spectrum Version 11.2.0.780 (Aperio Technologies, Inc.) and Aperio ImageScope

368   was used for annotation and to quantify cell populations. Cell counts were obtained using a

369   nuclear algorithm on Aperio ScanScope software and are reported as cells/mm^2.

Phenotypic analysis by flow cytometry

371   At necropsy, ~2 g of gently rinsed cecal tissue was placed in complete RPMI (RPMI

372   1640 [Life Technologies; Grand Island, NY] supplemented with 10% fetal calf serum [FCS,

373   Omega Scientific; Tarzana, CA], L-glutamine [Life Technologies], 25 mM HEPES [Sigma; St.

374   Louis, MO], essential amino acids and antibiotics [Sigma]) and stored on ice until processing. A

375   previously described protocol was adapted for isolation of both epithelial cells and lamina

376   propria cells from cecal tissue (39), with some modifications (Supplementary Information). Cells

377   from peripheral blood and ileocecal lymph nodes were isolated as previously described (40).

378   Approximately 10^6 cells per tissue were used for flow cytometric analysis.

379   Cells were stained with Zombie Yellow Viability dye (Biolegend, San Diego, CA),

380   followed by incubation with fluorescently-conjugated anti-porcine monoclonal antibodies (BD

381   Biosciences, San Jose, CA (except as noted)). Antibodies used included anti-porcine CD3 (clone

382   BB23-8E6-8C6), CD4 (clone 74-12-4), CD8α (clone 76-2-11), CD25 (clone K231.3B2,

383   Southern Biotech), γδTCR (clone MAC320), and FOXP3 (clone FJK16s). For staining of FoxP3

384   the Intracellular Nuclear Staining Kit (Biolegend) was used. Data were acquired on a BD LSRII

385   instrument and analyzed with FlowJo Software (FlowJo LLC, Ashland, Oregon). Representative

386   flow plots and gating strategy are available (Figures S1 and S2).

387   *RNA extraction, cDNA synthesis, and RT-qPCR of cecal tissue*

388   Host RNA was extracted using the TriReagent (Life Technologies)-modified protocol

389   with the PowerLyzer UltraClean Tissue & Cells RNA Isolation Kit (MoBio Laboratories, Inc.).

390   Homogenization in TriReagent was carried out in a Thermo Savant FastPrep® FP120 Cell

391   Disrupter (Qbiogene, Inc., Carlsbad, CA). An on-column DNAse step was included (On-Spin

392   Column DNase I Kit, Mo Bio Laboratories, Inc.). QuantiTect Reverse Transcription Kit

393   (Qiagen, Valencia, CA) was used for cDNA synthesis.

394   Gene expression was measured using the TaqMan® Universal Master Mix II system

395   (Applied Biosystems, Foster City, CA). Cycling conditions were 40 cycles of 95°C for 15 sec

396   and 60°C for 1 minute. The gene β-actin was used to normalize the expression of target genes

397   according to the $2^{-\Delta\Delta Cq}$ method (41). Primers and probes are described in Table S2.

398   *Microbial community analysis*

399   Microbial nucleic acids were extracted from feces and cecal contents using the

400   PowerMag fecal DNA/RNA extraction kit (MoBio). Only cecal contents were used for RNA

401   isolation. RNA samples were treated with DNase Max (MoBio) kit, and converted to cDNA

402   using the High Capacity cDNA Synthesis Kit (Applied Biosystems). Amplicons of the V4

403   region were generated and sequenced in accordance with the protocol from Kozich et al. (42).

404   Amplicons of the butyryl-CoA:acetate CoA transferase (*but*) gene were generated and sequenced

405   using the protocol from Trachsel et al., 2016 (43). Normalized pools for the 16S rRNA gene

406   library and *but* gene libraries were sequenced on a MiSeq (Illumina) using 2x250 V2 and 2x300

407   V3 chemistry, respectively.

IgA measurements

409   Cecal contents (~250 mg) were lyophilized, resuspended in extraction buffer (10mM

410   Tris, 100mM NaCl, 1mM $CaCl_2$, 0.5% Tween-20, 1 tablet cOmplete™, EDTA-free Protease

411   Inhibitor Cocktail (Roche, Branford, CT) per 100 mL) at 1mL extraction buffer per 30 mg

412   freeze-dried cecal contents, and vortexed on high for 10 minutes. Debris was pelleted by

413   centrifugation at 5000 x g and dilutions of the supernatant were used in the Pig IgA ELISA

414   Quantitation kit (Bethyl Laboratoties, Montgomery, TX). Results are reported as ng IgA/mg dry

415   contents.

Short-chain fatty acid (SCFA) measurements

417   One gram of material (cecal contents or feces) was suspended in 2 mL PBS, vortexed for

418   one minute, and debris was pelleted by centrifugation at 5000 x g for 10 minutes. Supernatant (1

419   mL) was added to heptanoic acid internal standards. Butylated fatty acid esters were generated

420   as described (44), and analyzed using an Agilent 7890 GC (Agilent, Santa Clara, CA).

Data analysis

422   Unless otherwise stated, Wilcoxon tests were used to test for statistical differences. Both

423   the 16S rRNA gene and *but* gene amplicon data were clustered into operational taxonomic units

424   (OTUs) with 97% similarity in mothur using the Miseq SOP (45). 16S rRNA gene sequences

425   were aligned to the SILVA reference alignment, and *but* sequences were aligned to an alignment

426   of *but* reference sequences downloaded from RDP's fungene database (46). Error rates

427 calculated by sequencing mock communities (47) for 16S rRNA genes and *but* genes were 1.3e-

428 06 and 2.2e-03 errors per basecall, respectively.

429   The R package vegan (48) was used to carry out ecological analyses. Community

430 structure similarity analyses were performed by calculating Bray-Curtis dissimilarities, and

431 statistical testing was accomplished using vegan's adonis and betadisper functions. Differential

432 abundance was determined using the DeSeq2 package (49). Correlations for network analysis

433 were calculated with CCREPE (50) for compositional data or the rcorr function from the hmsic

434 R package. Network layout was performed with the geomnet R package (30). Only significant,

435 positive correlations with a Spearman coefficient of at least 0.6 are shown.

436 **Data availability**

437   Raw sequence data is available in the SRA under project accession number

438 PRJNA476557. All processed data and R scripts used in this analysis are available at

439 https://github.com/Jtrachsel/RPS-2017.

440

441 **Acknowledgements**

442   We are grateful to the NADC animal care staff for their efforts. We thank Jennifer Jones,

443 Zahra Olson, Nicole Hasstedt, and Sam Humphrey for technical assistance, and Haley Jeppson

444 for help with R coding and figure consultation. Mention of trade names or commercial products

445 in this publication is solely for the purpose of providing specific information and does not imply

446 recommendation or endorsement by the U.S Department of Agriculture. USDA is an equal

447 opportunity provider and employer.

448   **Author Contributions:**

449   JT, CL, and HKA conceived of and planned the study. NG formulated and prepared the diets,

450   and provided guidance on diet phases. CL and CB collected the gene expression, flow cytometry,

451   IgA, and immunohistochemistry data. JT collected microbial community data and SCFA data.

452   JT performed the data analysis. JT, CB, HKA, and CL wrote and revised the manuscript.

453   **Figure Captions**

454   **Figure 1: A:** PERMANOVA pseudo F statistic over time for both the 16S- and *but* gene-based

455   fecal bacterial community analyses. A Bray-Curtis dissimilarity matrix was calculated from

456   OTUs clustered at 97% identity, and this dissimilarity matrix was used as the input for the

457   PERMANOVA tests. Each data point represents the PERMANOVA test statistic (F: intergroup

458   dissimilarity / intragroup dissimilarity) comparing the CON and RPS fecal bacterial community

459   structure at each time point; higher values equate to greater differences between treatment

460   groups. P-values are shown when $p < 0.05$. **B:** Group dispersion over time. Higher values on the

461   Y axis indicate that communities within that group are more dissimilar from each other. Lower

462   Y axis values indicate that communities in that group are more similar to each other. Error bars

463   represent the standard error around the mean.

464   **Figure 2:** Bacterial community structure and SCFA production in RPS-fed pigs (orange)

465   compared to CON-fed pigs (green) at day 21. Nonmetric multidimensional scaling (NMDS)

466   ordinations of 16S rRNA gene-based Bray-Curtis dissimilarities calculated from OTUs clustered

467   at 97% identity (**A**) and *but* gene-based Bray-Curtis dissimilarities calculated from OTUs

468   clustered at 97% identity (**B**). Points indicate group centroids, from discrete gut locations as

469   labeled. Centroids represent the approximate average community composition, and ellipses

470   show standard error around this average. 'Cec_cont_RNA'= RNA from cecal contents. **C:**

471   SCFA concentrations (mM) from cecal contents and feces at day 21 post-weaning.

472   **Figure 3:** Significantly (p<0.05) Differentially abundant genera based on 16S rRNA gene

473   sequences from the ileal mucosa (**A**), cecal mucosa (**B**), colonic mucosa (**C**), and feces (**D**) as

474   determined by DeSeq2. OTUs clustered at 97% similarity were combined by taxonomic

475   classification at the genus level. The results shown are $\log_2$ fold change between the CON

476   (control; green) and RPS (resistant potato starch; orange)-fed groups; note that the x-axis scale is

477   different for each panel. Positive log-fold changes indicate that a genus is enriched in the RPS

478   group, while negative log-fold changes indicate that a genus is enriched in the CON group. The

479   SILVA classification for each genus is labeled on the figure using both the family and genus

480   name. Genera shown in bold are those that harbor species with the capacity for respiration.

481   **Figure 4:** The abundance of OTU0087 over time (**A**) and in intestinal tissues at day 21 (**B**) in

482   CON (green) or RPS (orange)-fed pigs. 16S rRNA gene sequences from this OTU most closely

483   matched those from *Clostridium chartatabidum*, a member of the genus *Clostriduim sensu*

484   *stricto 1*. Bacteria similar to this organism have been isolated from chemostats fed with resistant

485   starch and inoculated with human feces (17).

486   **Figure 5:** Differentially abundant *but* gene OTUs from the ileal mucosa (**A**), cecal mucosa (**B**),

487   colonic mucosa (**C**), and feces (**D**) as determined by DeSeq2. The results shown are $\log_2$-fold

488   change between the CON (control) and RPS (resistant potato starch)-fed pigs; note that the x-

489   axis scale is different for each panel. Positive log-fold changes indicate that an OTU is enriched

490   in the RPS-fed animals, while negative log-fold changes indicate that an OTU is enriched in the

491   CON animals. OTUs were clustered at 97% similarity and are labeled with the species name for

492   their top BLAST hit followed by the percent identity for that hit. OTUs labeled in bold are those

493   that were consistently enriched in one treatment group or the other.

494   **Figure 6:** A network depicting correlations between 16S rRNA gene and *but* gene OTUs in the

495   fecal microbiota from RPS and CON fed animals calculated with CCREPE. Only significant (p

496   < 0.05) and positive correlations with a spearman correlation coefficient of at least 0.6 are

497   shown. The network was filtered to only include OTUs that were enriched in one treatment or

498   the other, and colors around the nodes indicate which treatment group that particular feature was

499   enriched in as determined by DeSeq2 (CON=green; RPS=orange). Nodes representing 16S

500   rRNA gene OTUs (97% similarity) are labeled with their taxonomic classification according to

501   the SILVA database. Labels are genus names except when classification at the genus level was

502   not possible, in which case family names are shown. Nodes representing *but* gene OTUs (97%

503   similarity) are labeled according to the species name of their closest BLAST hit.

504   **Figure 7:** Differences in T cell populations between the RPS and CON animals at 21 days post-

505   weaning. **A**) NMDS ordination of Bray-Curtis dissimilarities of T cell communities in various

506   tissues. Each point represents the total T cell community for one pig in a certain tissue, and

507   distances between points represent the similarities between communities.   **B**) The evenness

508   (Pielou's J) of the T cell communities in various tissues. Low evenness indicates that a

509   community is dominated by a few abundant members. **C**) Boxplots of significantly differentially

510   abundant T cell types from the cecal T cell community.

511   **Figure 8:** Differences in host traits associated with mucosal barrier function between CON and

512   RPS-fed animals. **A**) mRNA expression of barrier function-associated genes from the cecal

513   mucosa. **B**) Amount of IgA in cecal contents. Wilcoxon pvalues: DEFB1 p=0.16, IL-6 p=0.05,

514   MUC2 p=0.05, IgA p=0.01. DEFB1= beta defensin 1, IL-6=Interleukin 6 gene, MUC2=mucin 2

515   gene. IgA=Immunoglobulin A.

516   **Figure 9:** A network depicting correlations among cecal immune cells, 16S rRNA gene OTUs,

517   cecal SCFA concentrations, cecal host mRNA expression, and cecal IgA concentrations. Only

518   positive correlations are shown with a Spearman coefficient >0.6 and a p-value < 0.05. Bacterial

519   nodes are OTUs labeled with their taxonomic classification according to the SILVA database.

520   Labels are genus names except when no classification at the genus level was possible, in which

521   case family names are shown. Nodes shades with green are features that are significantly

522   enriched in the CON group, nodes shaded in orange are those significantly enriched in the RPS

523   group.

524

525   **Citations**

526   1.   Heo JM, Opapeju FO, Pluske JR, Kim JC, Hampson DJ, Nyachoti CM. 2013. Gastrointestinal health
527   and function in weaned pigs: a review of feeding strategies to control post-weaning diarrhoea
528   without using in-feed antimicrobial compounds. J Anim Physiol Anim Nutr (Berl) 97:207-37.
529   2.   Umu OC, Frank JA, Fangel JU, Oostindjer M, da Silva CS, Bolhuis EJ, Bosch G, Willats WG, Pope
530   PB, Diep DB. 2015. Resistant starch diet induces change in the swine microbiome and a
531   predominance of beneficial bacterial populations. Microbiome 3:16.
532   3.   Desai MS, Seekatz AM, Koropatkin NM, Kamada N, Hickey CA, Wolter M, Pudlo NA, Kitamoto S,
533   Terrapon N, Muller A, Young VB, Henrissat B, Wilmes P, Stappenbeck TS, Núñez G, Martens EC.
534   2016. A Dietary Fiber-Deprived Gut Microbiota Degrades the Colonic Mucus Barrier and
535   Enhances Pathogen Susceptibility. Cell 167:1339-1353.e21.
536   4.   Kelly CJ, Zheng L, Campbell EL, Saeedi B, Scholz CC, Bayless AJ, Wilson KE, Glover LE, Kominsky
537   DJ, Magnuson A, Weir TL, Ehrentraut SF, Pickel C, Kuhn KA, Lanis JM, Nguyen V, Taylor CT,
538   Colgan SP. 2015. Crosstalk between Microbiota-Derived Short-Chain Fatty Acids and Intestinal
539   Epithelial HIF Augments Tissue Barrier Function. Cell Host Microbe 17:662-71.
540   5.   den Besten G, van Eunen K, Groen AK, Venema K, Reijngoud DJ, Bakker BM. 2013. The role of
541   short-chain fatty acids in the interplay between diet, gut microbiota, and host energy
542   metabolism. J Lipid Res 54:2325-40.
543   6.   Kim M, Qie Y, Park J, Kim CH. 2016. Gut Microbial Metabolites Fuel Host Antibody Responses.
544   Cell Host Microbe 20:202-14.

545 7.   Rivera-Chavez F, Zhang LF, Faber F, Lopez CA, Byndloss MX, Olsan EE, Xu G, Velazquez EM,
546   Lebrilla CB, Winter SE, Baumler AJ. 2016. Depletion of butyrate-producing *Clostridia* from the
547   gut microbiota drives an aerobic luminal expansion of *Salmonella*. Cell Host Microbe 19:443-54.
548 8.   Spees AM, Lopez CA, Kingsbury DD, Winter SE, Baumler AJ. 2013. Colonization resistance: battle
549   of the bugs or me´nage a`trois with the host? PLOS Pathogens 9:1-4.
550 9.   Rivera-Chavez F, Winter SE, Lopez CA, Xavier MN, Winter MG, Nuccio SP, Russell JM, Laughlin
551   RC, Lawhon SD, Sterzenbach T, Bevins CL, Tsolis RM, Harshey R, Adams LG, Baumler AJ. 2013.
552   *Salmonella* uses energy taxis to benefit from intestinal inflammation. PLoS Pathog 9:e1003267.
553 10. Xiong H, Guo B, Gan Z, Song D, Lu Z, Yi H, Wu Y, Wang Y, Du H. 2016. Butyrate upregulates
554   endogenous host defense peptides to enhance disease resistance in piglets via histone
555   deacetylase inhibition. Sci Rep 6:27070.
556 11. Harrison OJ, Powrie FM. 2013. Regulatory T cells and immune tolerance in the intestine. Cold
557   Spring Harb Perspect Biol 5.
558 12. Heo JM, Agyekum AK, Yin YL, Rideout TC, Nyachoti CM. 2014. Feeding a diet containing resistant
559   potato starch influences gastrointestinal tract traits and growth performance of weaned pigs.
560   Journal Of Animal Science 92:3906-3913.
561 13. Ravcheev DA, Thiele I. 2014. Systematic genomic analysis reveals the complementary aerobic
562   and anaerobic respiration capacities of the human gut microbiota. Frontiers in Microbiology
563   5:674.
564 14. Yamamoto Y, Poyart C, Trieu-Cuot P, Lamberet G, Gruss A, Gaudu P. 2005. Respiration
565   metabolism of Group B Streptococcus is activated by environmental haem and quinone and
566   contributes to virulence. Mol Microbiol 56:525-34.
567 15. Sellars MJ, Hall SJ, Kelly DJ. 2002. Growth of Campylobacter jejuni supported by respiration of
568   fumarate, nitrate, nitrite, trimethylamine-N-oxide, or dimethyl sulfoxide requires oxygen. J
569   Bacteriol 184:4187-96.
570 16. Loy A, Pfann C, Steinberger M, Hanson B, Herp S, Brugiroux S, Gomes Neto JC, Boekschoten MV,
571   Schwab C, Urich T, Ramer-Tait AE, Rattei T, Stecher B, Berry D. 2017. Lifestyle and Horizontal
572   Gene Transfer-Mediated Evolution of Mucispirillum schaedleri, a Core Member of the Murine
573   Gut Microbiota. mSystems 2.
574 17. Sharp R, Macfarlane GT. 2000. Chemostat Enrichments of Human Feces with Resistant Starch
575   Are Selective for Adherent Butyrate-Producing Clostridia at High Dilution Rates. Applied and
576   Environmental Microbiology 66:4212-4221.
577 18. Venkataraman A, Sieber JR, Schmidt AW, Waldron C, Theis KR, Schmidt TM. 2016. Variable
578   responses of human microbiomes to dietary supplementation with resistant starch. Microbiome
579   4:33.
580 19. Ravcheev DA, Gerasimova AV, Mironov AA, Gelfand MS. 2007. Comparative genomic analysis of
581   regulation of anaerobic respiration in ten genomes from three families of gamma-
582   proteobacteria (Enterobacteriaceae, Pasteurellaceae, Vibrionaceae). BMC Genomics 8:54.
583 20. Cushing K, Alvarado DM, Ciorba MA. 2015. Butyrate and Mucosal Inflammation: New Scientific
584   Evidence Supports Clinical Observation. Clin Trans Gastroenterol 6:e108.
585 21. Bourriaud C, Robins RJ, Martin L, Kozlowski F, Tenailleau E, Cherbut C, Michel C. 2005. Lactate is
586   mainly fermented to butyrate by human intestinal microfloras but inter-individual variation is
587   evident. Journal of Applied Microbiology 99:201-212.
588 22. Kim JC, Hansen CF, Mullan BP, Pluske JR. 2012. Nutrition and pathology of weaner pigs:
589   Nutritional strategies to support barrier function in the gastrointestinal tract. Animal Feed
590   Science and Technology 173:3-16.
591 23. Zeng H, Chi H. 2015. Metabolic control of regulatory T cell development and function. Trends
592   Immunol 36:3-12.

593 24. Schilderink R, Verseijden C, Seppen J, Muncan V, Brink GRvd, Lambers TT, Tol EAv, Jonge WJd.
594   2016. The SCFA butyrate stimulates epithelial production of retinoic acid via inhibition of
595   epithelial HDAC. Am J Physiol Gastrointest Liver Physiol 310:G1138-G1146.
596 25. Holman DB, Brunelle BW, Trachsel J, Allen HK. 2017. Meta-analysis To Define a Core Microbiota
597   in the Swine Gut. mSystems 2.
598 26. Le Leu RK, Hu Y, Brown IL, Woodman RJ, Young GP. 2010. Synbiotic intervention of
599   Bifidobacterium lactis and resistant starch protects against colorectal cancer development in
600   rats. Carcinogenesis 31:246-51.
601 27. Accetto T, Avgustin G. 2015. Polysaccharide utilization locus and CAZYme genome repertoires
602   reveal diverse ecological adaptation of Prevotella species. Syst Appl Microbiol 38:453-61.
603 28. Fouhse JM, Ganzle MG, Regmi PR, van Kempen TA, Zijlstra RT. 2015. High Amylose Starch with
604   Low In Vitro Digestibility Stimulates Hindgut Fermentation and Has a Bifidogenic Effect in
605   Weaned Pigs. J Nutr doi:10.3945/jn.115.214353.
606 29. Yu Q, Zhang S, Li L, Xiong L, Chao K, Zhong B, Li Y, Wang H, Chen M. 2015. Enterohepatic
607   Helicobacter Species as a Potential Causative Factor in Inflammatory Bowel Disease: A Meta-
608   Analysis. Medicine (Baltimore) 94:e1773.
609 30. Tyner S, Briatte F, Hofmann H. 2017. Network Visualization with ggplot. The R Journal.
610 31. Belenguer A, Duncan SH, Holtrop G, Anderson SE, Lobley GE, Flint HJ. 2007. Impact of pH on
611   lactate formation and utilization by human fecal microbial communities. Appl Environ Microbiol
612   73:6526-33.
613 32. Suzuki K, Ha SA, Tsuji M, Fagarasan S. 2007. Intestinal IgA synthesis: a primitive form of adaptive
614   immunity that regulates microbial communities in the gut. Semin Immunol 19:127-35.
615 33. Kubinak JL, Petersen C, Stephens WZ, Soto R, Bake E, O'Connell RM, Round JL. 2015. MyD88
616   signaling in T cells directs IgA-mediated control of the microbiota to promote health. Cell Host
617   Microbe 17:153-63.
618 34. Churlaud G, Pitoiset F, Jebbawi F, Lorenzon R, Bellier B, Rosenzwajg M, Klatzmann D. 2015.
619   Human and Mouse CD8+CD25+FOXP3+ Regulatory T Cells at Steady State and during
620   Interleukin-2 Therapy. Frontiers in Immunology 6.
621 35. Rooks MG, Veiga P, Wardwell-Scott LH, Tickle T, Segata N, Michaud M, Gallini CA, Beal C, van
622   Hylckama-Vlieg JE, Ballal SA, Morgan XC, Glickman JN, Gevers D, Huttenhower C, Garrett WS.
623   2014. Gut microbiome composition and function in experimental colitis during active disease
624   and treatment-induced remission. ISME J 8:1403-17.
625 36. Dubois A, Borén T. 2007. Helicobacter pylori is invasive and it may be a facultative intracellular
626   organism. Cellular microbiology 9:1108-1116.
627 37. McCracken BA, Spurlock ME, Mark A R, Zuckermann FA, Gaskins HR. 1999. Weaning Anorexia
628   May Contribute to Local Inflammation in the Piglet Small Intestine. Journal of Nutrition 129:613-
629   619.
630 38. Pahar B, Lackner AA, Veazey RS. 2006. Intestinal double-positive CD4+CD8+ T cells are highly
631   activated memory cells with an increased capacity to produce cytokines. Eur J Immunol 36:583-
632   92.
633 39. Goodyear AW, Kumar A, Dow S, Ryan EP. 2014. Optimization of murine small intestine leukocyte
634   isolation for global immune phenotype analysis. J Immunol Methods 405:97-108.
635 40. Sandbulte MR, Platt R, Roth JA, Henningson JN, Gibson KA, Rajao DS, Loving CL, Vincent AL.
636   2014. Divergent immune responses and disease outcomes in piglets immunized with inactivated
637   and attenuated H3N2 swine influenza vaccines in the presence of maternally-derived antibodies.
638   Virology 464-465:45-54.
639 41. Livak KJ, Schmittgen TD. 2001. Analysis of relative gene expression data using real-time
640   quantitative PCR and the 2(-Delta Delta C(T)) Method. Methods 25:402-8.

641 42. Kozich JJ, Westcott SL, Baxter NT, Highlander SK, Schloss PD. 2013. Development of a dual-index
642   sequencing strategy and curation pipeline for analyzing amplicon sequence data on the MiSeq
643   Illumina sequencing platform. Appl Environ Microbiol 79:5112-20.
644 43. Trachsel J, Bayles DO, Looft T, Levine UY, Allen HK. 2016. Function and Phylogeny of Bacterial
645   Butyryl Coenzyme A:Acetate Transferases and Their Diversity in the Proximal Colon of Swine.
646   Appl Environ Microbiol 82:6788-6798.
647 44. Salanitro JP, Muirhead PA. 1975. Quantitative Method for the Gas Chromatographic Analysis of
648   Short-Chain Monocarboxylic and Dicarboxylic Acids in Fermentation Media. Applied
649   Microbiology 29:374-381.
650 45. Schloss PD, Westcott SL, Ryabin T, Hall JR, Hartmann M, Hollister EB, Lesniewski RA, Oakley BB,
651   Parks DH, Robinson CJ, Sahl JW, Stres B, Thallinger GG, Van Horn DJ, Weber CF. 2009.
652   Introducing mothur: open-source, platform-independent, community-supported software for
653   describing and comparing microbial communities. Appl Environ Microbiol 75:7537-41.
654 46. Fish JA, Chai B, Wang Q, Sun Y, Brown CT, Tiedje JM, Cole JR. 2013. FunGene: the functional
655   gene pipeline and repository. Front Microbiol 4:291.
656 47. Allen HK, Bayles DO, Looft T, Trachsel J, Bass BE, Alt DP, Bearson SMD, Nicholson T, Casey TA.
657   2016. Pipeline for amplifying and analyzing amplicons of the V1–V3 region of the 16S rRNA gene.
658   BMC Research Notes 9.
659 48. Jari Oksanen, F. Guillaume Blanchet, Michael Friendly, Roeland Kindt, Pierre Legendre, Dan
660   McGlinn, Peter R. Minchin, R. B. O'Hara, Gavin L. Simpson, Peter Solymos, M. Henry H. Stevens,
661   Eduard Szoecs, Helene Wagner. 2017. vegan: Community Ecology Package, vR package version
662   2.4-2. https://CRAN.R-project.org/package=vegan.
663 49. Love MI, Huber W, Anders S. 2014. Moderated estimation of fold change and dispersion for
664   RNA-seq data with DESeq2. Genome Biology 15:550.
665 50. Emma schwager, Craig B, Weingart G. 2014. ccrepe: ccrepe_and_nc.score, vR package version
666   1.12.1.
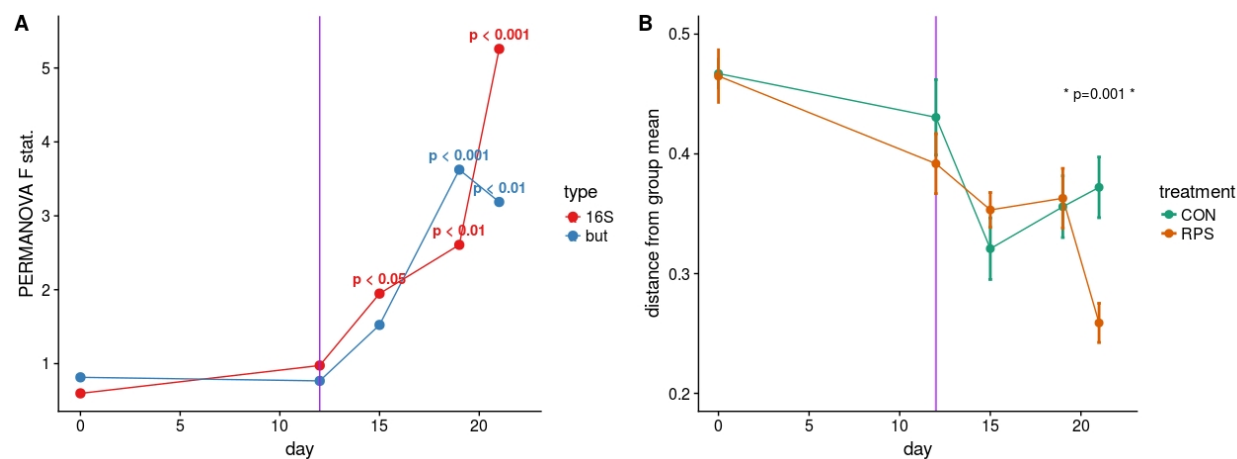
667

668

669

670

671

672

673

674

675

Figure 1: A: PERMANOVA pseudo F statistic over time for both the 16S- and *but* gene-based fecal microbial community analyses. A Bray-Curtis dissimilarity matrix was calculated from OTUs clustered at 97% identity, and this dissimilarity matrix was used as the input for the PERMANOVA tests. Each data point represents the PERMANOVA test statistic (F: intergroup dissimilarity / intragroup dissimilarity) comparing the CON and RPS fecal bacterial community structure at each time point; higher values equate to greater differences between treatment groups. P-values are shown when $p < 0.05$. **B:** Group dispersion over time. Higher values on the Y axis indicate that communities within that group are more dissimilar from each other. Lower Y axis values indicate that communities in that group are more similar to each other. Error bars represent the standard error around the mean.
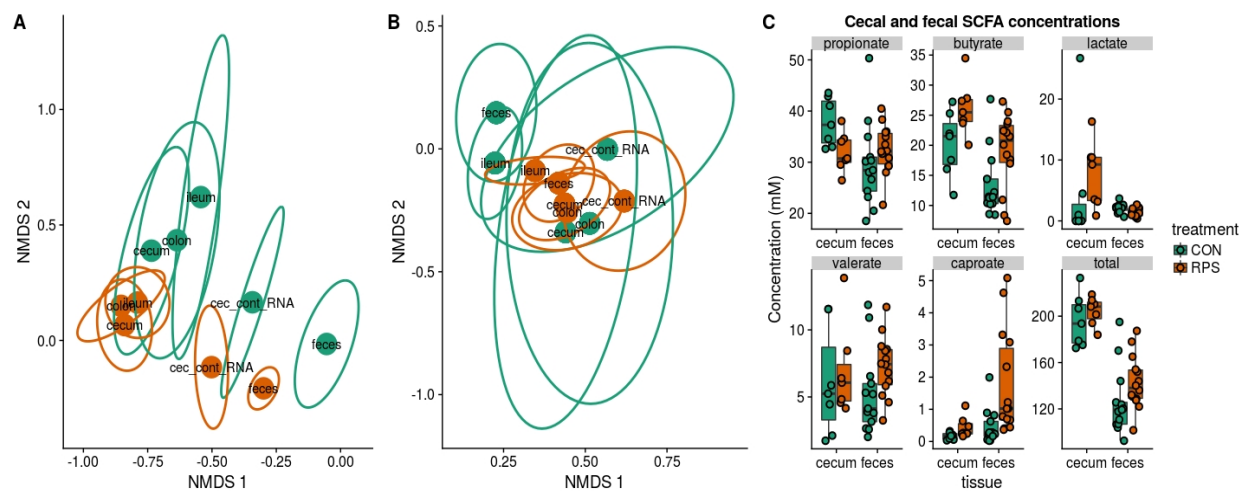
680

681

682

683

684

685

Figure 2: Nonmetric multidimensional scaling (NMDS) ordinations of 16S rRNA gene-based Bray-Curtis dissimilarities (A) and *but* gene-based Bray-Curtis dissimilarities (B). Points indicate group centroids, from discrete gut locations as labeled. Centroids represent the approximate average community composition and ellipses show standard error around this average. 'Cec_cont_RNA'= RNA from cecal contents. C: SCFA concentrations (mM) from cecal contents and feces at day 21 post-weaning.
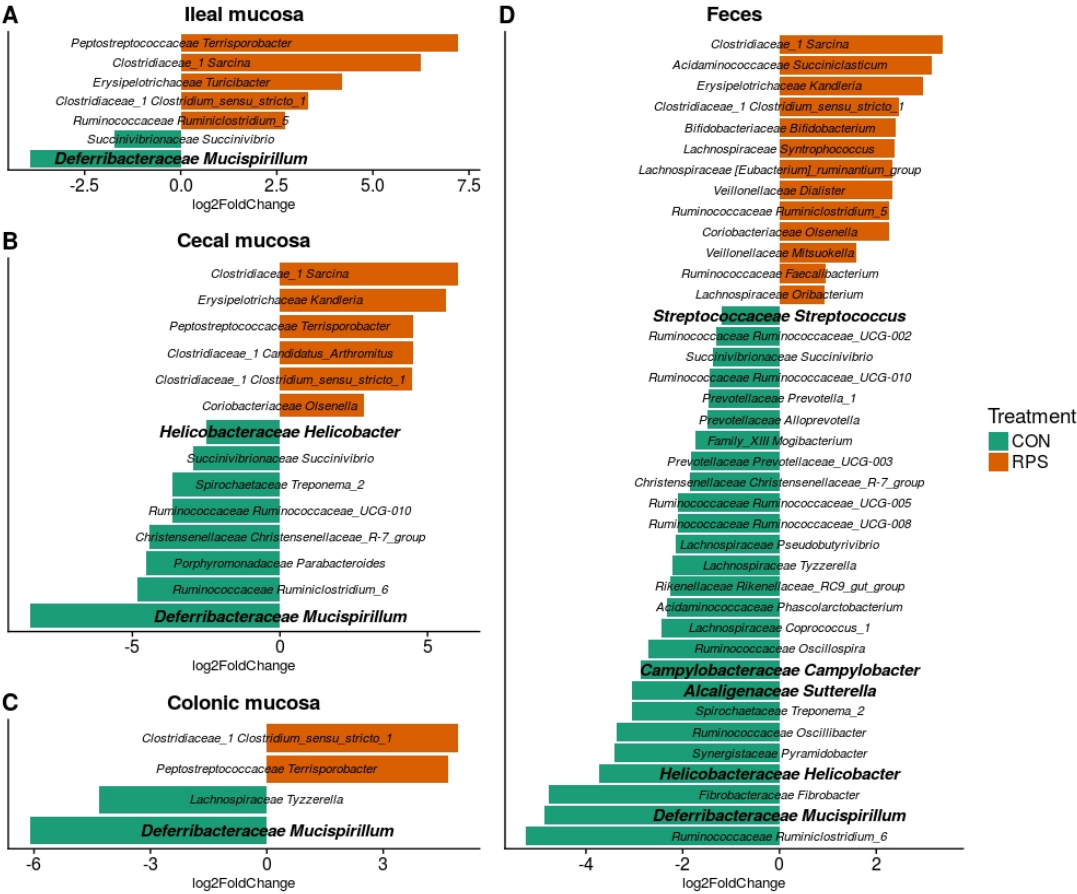
686

Figure 3: Differentially abundant genera based on 16S rRNA gene sequences from the ileal mucosa (A), cecal mucosa (B), colonic mucosa (C), and feces (D) as determined by DeSeq2. The results shown are log2 fold change between the CON (control) and RPS (resistant potato starch)-fed groups; note that the x-axis scale is slightly different for each panel. Positive log fold changes indicate that OTU is enriched in the RPS group while negative log fold changes indicate that OTU is enriched in the CON group OTUs clustered at 97% similarity were combined by taxonomic classification at the genus level. The SILVA classification for each genera is shown combining the family and genus name. Genera shown in bold are those which harbor species with the capacity for respiration.
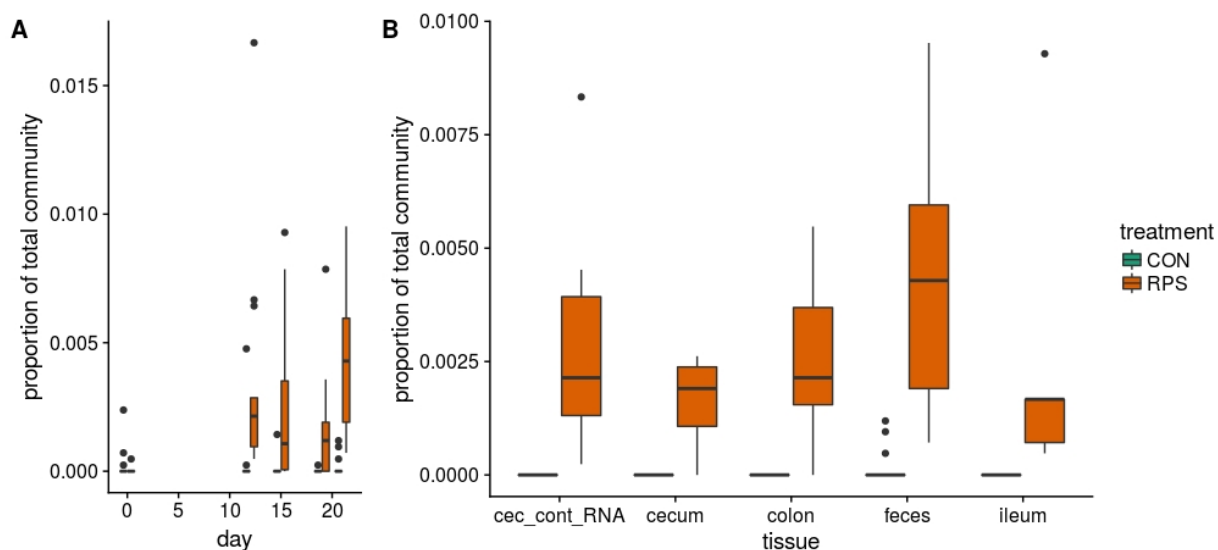
687

688

689

690

691

692

Figure 4: Boxplots of the abundance of OTU0087 over time (A), and in various tissues at day 21 (B). 16S rRNA gene sequences from this OTU most closely matched those from *Clostridium chartatabidum* a member of the genus *Clostriduim sensu stricto 1*. This OTU was detected mainly in pigs that were fed RPS though it was detected at low levels in the feces of CON pigs but not in any other tissue.
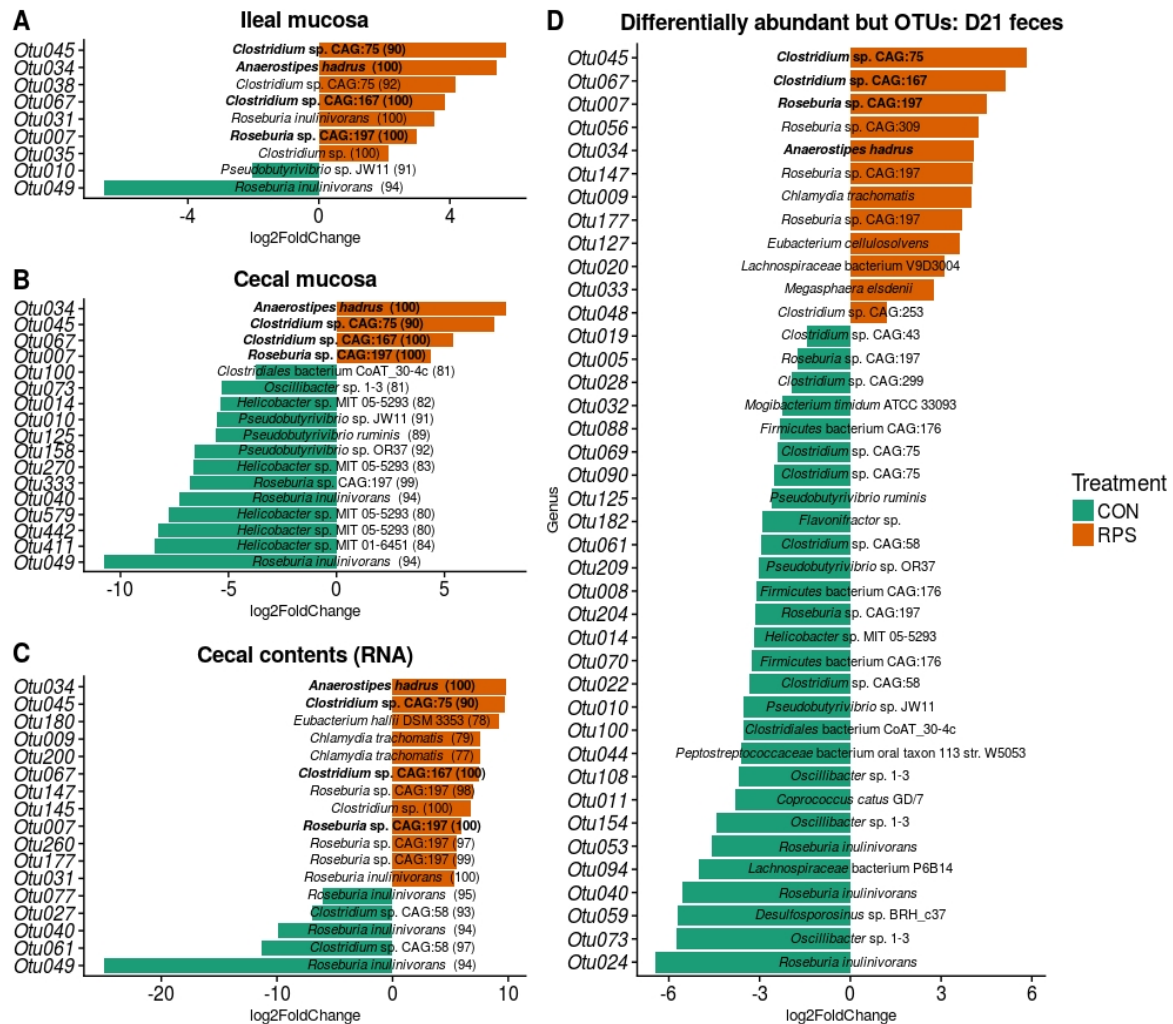
693

694

695

696

697

Figure 5: Significantly (p<0.05) differentially abundant but gene OTUs from the ileal mucosa (A), cecal mucosa (B), colonic mucosa (C), and feces (D) as determined by DeSeq2. The results shown are log2 fold change between the CON (control) and RPS (resistant potato starch)-fed groups; note that the x-axis scale is slightly different for each panel. Positive log fold changes indicate that OTU is enriched in the RPS group while negative log fold changes indicate that OTU is enriched in the CON group. OTUs were clustered at 97% similarity and are labeled with the species name for their closest BLAST hit followed by the percent identity for that hit. OTUs labeled in bold are those which were consistently enriched in one treatment group or the other.
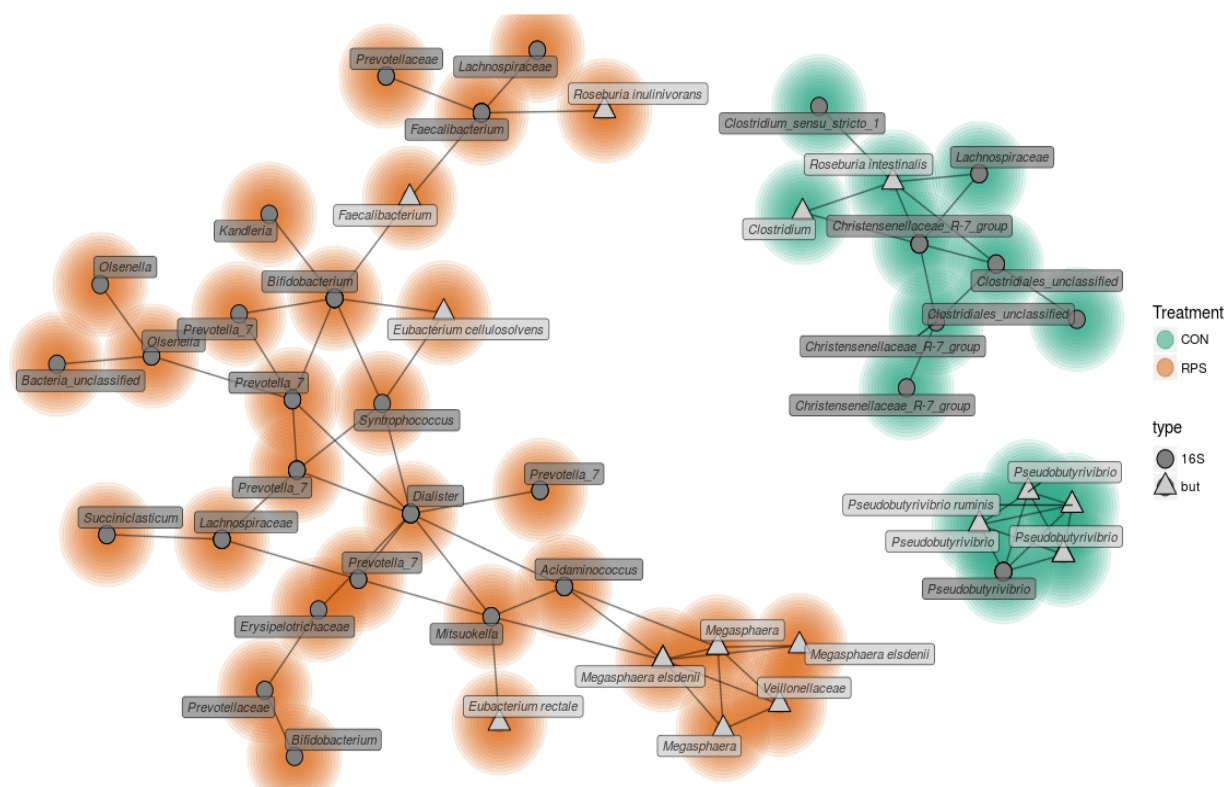
698

699

700

701

702

Figure 6: A network depicting correlations between 16S rRNA gene and *but* gene OTUs in the fecal microbiota calculated with CCREPE. Only significant (p < 0.05) positive correlations with a spearman correlation coefficient of at least 0.6 are shown. The network was filtered to only include OTUs which were enriched in one treatment or the other and colors around the nodes indicate which treatment group that particular feature was enriched in as determined by DeSeq2. 16S nodes are OTUs (97% similarity) labeled with their taxonomic classification according to the SILVA database, labels are genera names except when classification at the genera level was not possible, in which case family names are shown. *but* gene nodes are OTUs (97% similarity) labeled according to the species name of their closest BLAST hit.
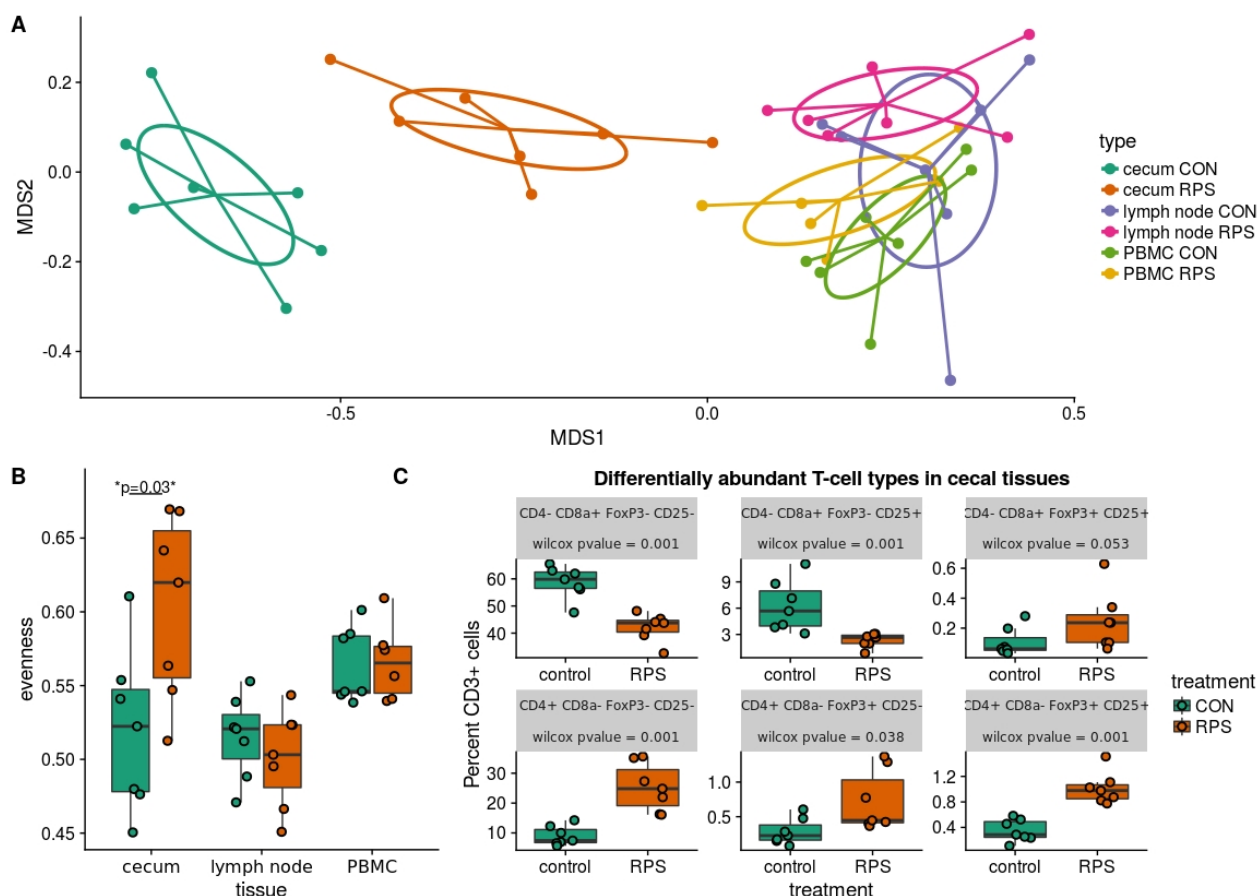
703

704

Figure 7A) A Bray-Curtis-based NMDS ordination of T cell communities in various tissues. Each point represents the total T cell community for one pig in a certain tissue and distances between points represent the similarities between communities. B) The evenness of the T cell communities in various tissues. Low evenness indicates that a community is dominated by a few abundant members C) boxplots of significantly differentially abundant T cell types from the cecal T cell community.

705

706

707

708

709

710

711

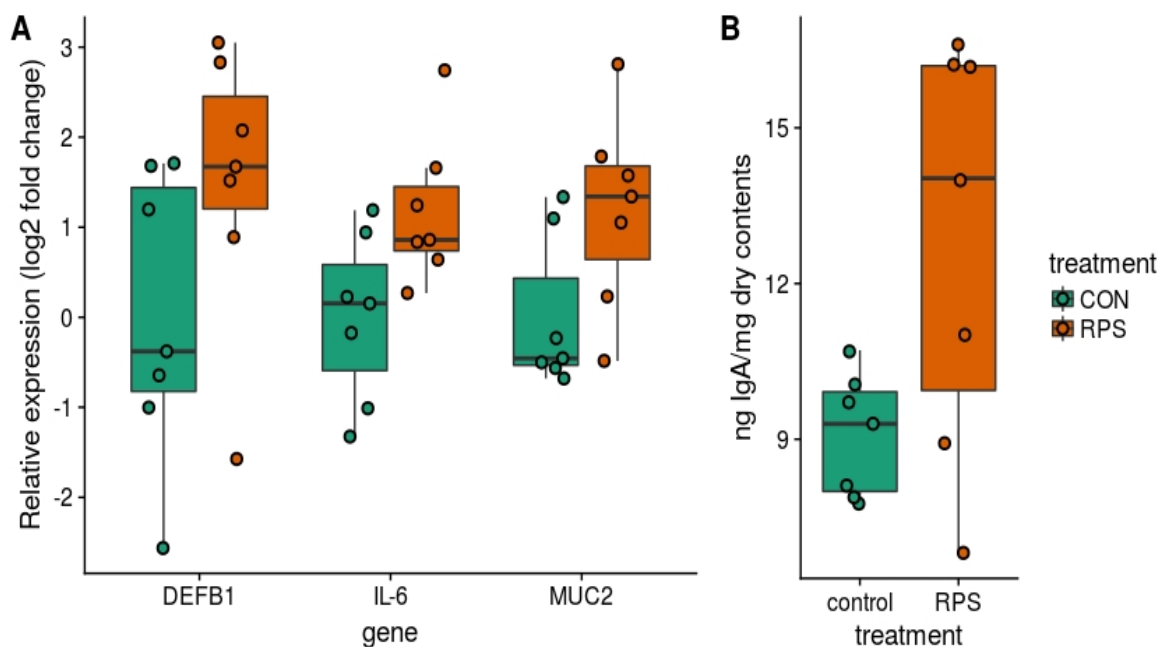**Figure 8: A)** mRNA expression of barrier function associated genes from the cecal mucosa. B) Amount of IgA in cecal contents. Wilcoxon pvalues: DEFB1 p=0.16, IL-6 p=0.05, MUC2 p=0.05, IgA p=0.01. DEFB1= beta defensin 1, IL-6=Interleukin 6 gene, MUC2=mucin 2 gene. IgA=Immunoglobulin A.

712

713

714

715

716

717

718

719

720

721

722

Figure 9: A network depicting correlations among immune cells, 16S rRNA gene OTUs, cecal SCFA concentrations, cecal host mRNA expression, and cecal IgA concentrations. Only positive correlations are shown with a Spearman coefficient >0.6 and a p-value < 0.05. Bacterial nodes are OTUs labeled with their taxonomic classification according to the SILVA database, labels are genera names except when no classification at the genera level was possible in which case family names are shown.

723